Nonlinear Multichannel Algorithms for Estimating Sea Surface Temperature with AVHRR Satellite Data

CHARLES C. WALTON

NOAA, Washington, DC

(Manuscript received 10 July 1986, in final form 18 June 1987)

ABSTRACT

The familiar linear multichannel sea surface temperature algorithms (MCSST) for estimating sea surface temperature with AVHRR satellite data describe the solution in terms of a constant gamma parameter multiplied by the measured brightness temperature difference of two of the window channels. A nonlinear algorithm is developed in this paper which is similar in form to the MCSST algorithm but with the gamma parameter having a specific two- or three-channel temperature dependence.

Simulation studies show that the linear and nonlinear algorithms provide nearly identical accuracies for a wide range of atmospheric conditions if the satellite data are error free. When random or noncorrelative error sources are present in the multichannel AVHRR data, it is found that the nonlinear algorithms significantly reduce their effect upon the final solution relative to the linear MCSST solution. These results are verified with actual AVHRR data obtained in January–March 1982 and 1983. The algorithm estimates of surface temperature are compared with buoy measurements in the North Atlantic and North Pacific.

1. Introduction

The theoretical basis of a multiple-window channel algorithm for estimating sea surface temperature with satellite infrared data was developed in the 1970s. A history of this development is given elsewhere (McMillin and Crosby, 1984). The theoretical development results in an algorithm of the form

$$\mathrm{SST} = T_j + \gamma(T_i - T_j), \tag{1}$$

where T_i and T_j are brightness temperature measurements at two different wavelengths in the 11–12 μm window spectral region. The gamma parameter, γ, is found to be constant under certain conditions and is given by

$$\gamma = k_j/(k_j - k_i), \tag{2}$$

where k_i and k_j are the water vapor absorption coefficients. The simplicity of this approach influenced the design of such instruments as the Advanced Very High Resolution Radiometer (AVHRR) on the TIROS-N series of satellites, which includes two or three window channels in the 3.7 μm and the 11–12 μm spectral regions (Schwalb, 1978). Indeed, since 1981 the National Environmental Satellite Data, and Information Service (NESDIS) has been operationally providing global maps of sea surface temperatures obtained with AVHRR-based Multi-Channel Sea Surface Temperature (MCSST) algorithms of the form given by (1). A comprehensive description of the operational algorithms is given by McClain et al. (1985), and global estimates of the accuracy achieved with these algorithms are very impressive (Strong and McClain, 1984).

Under very moist conditions, however, the simplifying assumptions leading to (1) are suspect. It is assumed that the atmospheric transmittance, τ_1, in channel i may be approximated by

$$\tau_1 \approx e^{-kx} \approx 1 - k_i X, \tag{3}$$

where X is the water vapor amount. A set of warm marine profiles with varying amounts of water vapor have been applied to a radiative transfer model (Weinreb and Hill, 1980) to estimate τ_1 for two spectral intervals (30 cm^{-1} width) near the center of the 11 and 12 μm channels of the AVHRR. The approximation given by (3) is applied to define the effective absorption coefficients k_i, and (2) yields the parameter γ, which is plotted against water vapor amount in Fig. 1. Clearly γ has a water vapor dependence (see also Dalu et al., 1981).

Additional problems appear in cold dry polar atmospheres. The absorption coefficient due to water vapor is considerably less in the 3.7 μm spectral window then at 11 or 12 μm, whereas absorption by uniformly mixed gases, i.e., CO_2, N_2, is much greater. Thus, the effective absorption coefficient at 3.7 μm, which includes the absorption by the mixed gases as well as water vapor and is defined with (3), changes from being less than to becoming greater than that at 11 μm as the water vapor amount decreases from a hot tropical

Corresponding author address: Dr. Charles C. Walton, NOAA, National Environmental Satellite, Data and Information Service, Washington, D.C. 20233.

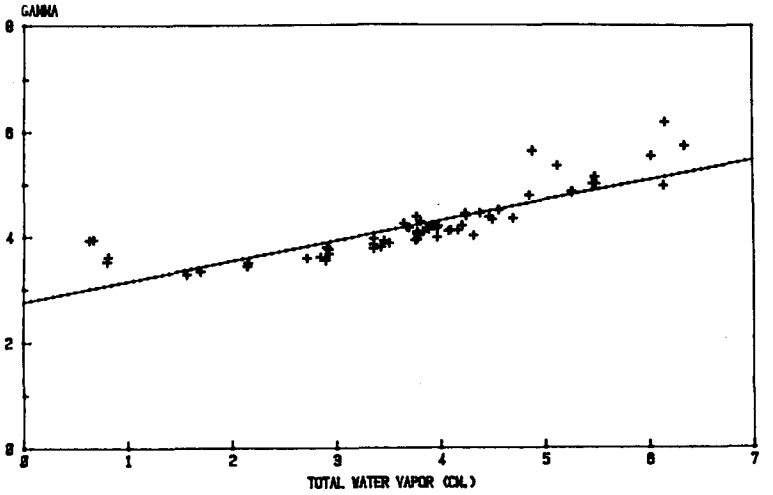

FIG. 1. The gamma parameter associated with two spectral intervals in the 11 to 12 μm region as a function of total atmospheric precipitable water. The data are computed with a radiative transfer model (Weinreb and Hill, 1980), which is applied to a set of 64 cloud-free marine soundings.

atmosphere to a dry polar atmosphere. Further, in dry polar atmospheres water vapor may be considered a uniform trace gas. Assuming no large air/sea temperature discontinuities, an adequate algorithm for correcting for absorption by uniform gases is

$$\mathrm{SST}_i = AT_i + B_i. \tag{4}$$

This latter solution, which can be obtained by linear regression with a diverse set of ground truth measurements and coincident single channel AVHRR temperature measurements, is preferable to (1) when error sources such as instrumental noise are significant because the parameter γ is normally considerably larger than the coefficient A, which is near unity.

The succeeding sections describe a nonlinear multichannel algorithm for estimating sea surface temperatures that can be described with (1) but where γ is a function of water vapor amount and temperature. At low temperatures the algorithm approaches a single channel solution similar to (4).

2. A graphical derivation

A simple graphical derivation of the MCSST algorithm given by (1) is possible. In this approach the brightness temperature in two different window channels (T_i) is plotted against the corresponding water vapor absorption coefficient (k_i), which is assumed to be a constant. The straight line connecting these two points is extrapolated to a zero absorption coefficient value. The corresponding temperature represents the solution. Graphical examples of this procedure are given in Prabhakara et al. (1974).

A similar graphical approach yields a decidedly nonlinear solution. The graphical representation is shown in Fig. 2. The single channel algorithm given by (4) is plotted against the corresponding brightness temperature in two different window channels. The line which connects the points (T_i, SST_i) and (T_j, SST_j) is extrapolated to intersect the equal temperature line (SST = T), which corresponds to a channel having no atmospheric absorption. The cross product sea surface temperature (CPSST) solution corresponding to this intersection point is obtained by equating the tangent of the two similar right triangles ACE and BCD yielding,

$$\mathrm{CPSST}\ (i, j) = \frac{T_i\mathrm{SST}_j - T_j\mathrm{SST}_i}{T_i - T_j + \mathrm{SST}_j - \mathrm{SST}_i}, \tag{5}$$

where i and j represent two separate window channels such as the 11 and 12 μm channels of the AVHRR. The single channel solution, SST_i, may be obtained by linear regression from a diverse set of marine atmospheres, but it will exhibit large errors in regions of high moisture variability. The graphical solution is represented in Fig. 2 for three different moisture conditions—very dry, average, and very moist. A physical justification for both the MCSST and CPSST algorithms is given in appendix A.

The graphical MCSST and CPSST solutions both involve a linear extrapolation assumption that may result in error. The solutions are made more flexible by allowing for a constant offset to one of the brightness temperatures of the form $T_i^* = T_i + C$. With this offset the MCSST solution becomes $T_j + \gamma(T_i - T_j) + \gamma C$, which is the usual multiple linear regression form of the MCSST solution. The effect of the temperature offset upon the CPSST solution is not so obvious, but is shown with the dashed lines in Fig. 2. In practice, the

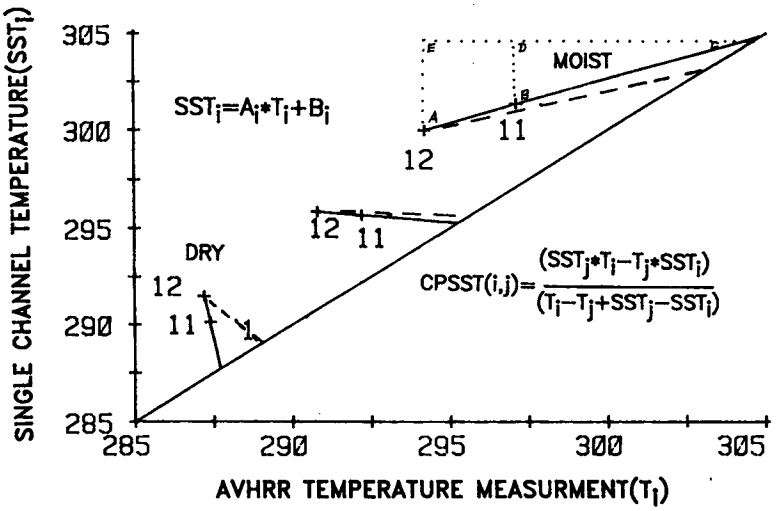

FIG. 2. A graphical representation of the nonlinear CPSST split-window algorithm. The single-channel solution, SST_i, is plotted as a function of the corresponding window-channel brightness temperature, T_i, for each of the two AVHRR split-window channels. The line connecting these points is extrapolated to the equal temperature point (solid line), which corresponds to a channel having no atmospheric absorption. The corresponding temperature is the solution. Results are shown for three different atmospheric conditions. The dashed lines show the effect of adding a constant offset to the 11 μm brightness temperature.

temperature offset is adjusted to minimize the error of the CPSST solution in a statistical sense. It is apparent from Fig. 2 that if $SST_i = SST_j$, which occurs only in average or climatological atmospheric conditions, then the CPSST solution is simply SST_i. Similarly if $T_i^* = T_j$, then the solution is T_i^*. The largest temperature correction for water vapor absorption occurs under very moist conditions when $T_i^* - T_j$ is large, although unlike the MCSST solution, the amount of correction is a function of the absolute temperatures as well as the temperature difference. The temperature dependence can be expressed mathematically by manipulating (5) into the form

$$\text{CPSST}(i,j) = \frac{SST_j - T_j}{SST_j - T_j + T_i^* - SST_i} \times (T_i^* - T_j) + T_j. \quad (6)$$

This form of the solution is identical to the MCSST solution, (1), although the gamma parameter has a specific two-channel temperature dependence. Mathematically (5) and (6) are identical and the temperature offset, T_i^*, can be applied to either equation.

3. Algorithm development with simulation data

Simulations of the influence of an aerosol-free atmosphere upon measurements in the three AVHRR window channels are performed using a procedure developed at NESDIS and detailed elsewhere (Weinreb and Hill, 1980). Using external radiosonde temperature and moisture profile data as input, the procedure numerically integrates the radiative transfer equation to estimate the radiance at the top of the atmosphere. The spectral bandpasses of the AVHRR channels are subdivided into 20 or 30 cm^{-1} subintervals, within which the radiative transfer equation is integrated separately through 100 pressure levels. The computed radiances at the top of the atmosphere in each subinterval are then weighted with the filter response of the AVHRR channel to provide the final wide-band radiance. The heart of the procedure is the calculation of atmospheric transmittances at each pressure level, which is described in detail in the previous reference. The calculation includes the effects of water vapor, molecular nitrogen, and the uniformly mixed gases CO_2, N_2O, CO, and CH_4. Specifically excluded are ozone, aerosols and water clouds. Also nonzero surface reflectivity effects are not included in this model.

The atmospheric transmittance model has been applied to a diverse set of 110 marine atmospheric profiles to determine cloud-free simulated brightness temperatures in each of the three AVHRR window channels on the NOAA-7 spacecraft. The set of marine profiles, which are obtained from radiosonde measurements, cover a large range of temperature and moisture conditions. It is similar to the set used to derive the operational MCSST algorithms used at NESDIS (McClain, 1981), but it includes a better representation of dry polar atmospheres. (Only three examples are included in the operational set of profiles.)

A simple linear regression of $(SST - T_i)$ vs $(T_i - T_j)$

provides various MCSST algorithms, where SST is the radiosonde-measured surface air temperature. The resulting dual-window (3, 4), split window (4, 5) and triple-window (3, 4, 5) algorithm are shown below:

$$\left.\begin{aligned} \text{MCSST (3, 4)} &= T_{11} + 1.616(T_{3.7} - T_{11}) + 1.07 \\ \text{MCSST (4, 5)} &= T_{12} + 3.15(T_{11} - T_{12}) + 0.10 \\ \text{MCSST (3, 4, 5)} &= T_{11} + 0.943(T_{3.7} - T_{12}) + 0.61 \end{aligned}\right\}. \quad (7)$$

The channel designations, i.e., 3, 4 and 5, refer to the three AVHRR window channels centered near 3.7, 11 and 12 μm (3.55–3.93, 10.3–11.3, and 11.5–12.5 μm), respectively. It may be noted that the coefficients associated with these algorithms are somewhat different than those generated operationally at NESDIS from a somewhat less diverse set of atmospheric profiles (Walton, 1985).

The procedure for deriving the CPSST algorithms involves two steps. First the single channel algorithms, (4), are computed by regressing SST against T_i. Next, the offset temperature, $T_i^* = T_i + C$, which minimizes the scatter of the CPSST algorithm relative to the actual surface temperature, SST, is computed by trial and error. Unlike the MCSST algorithms, linear regression will not yield this parameter for the CPSST algorithms. A nonlinear regression procedure for estimating this parameter is given in appendix B. Generally, the larger the positive offset, the smaller the effective gamma parameter becomes. As a result, the mean bias of the CPSST algorithms (<0.1°C) relative to the surface temperature is insensitive to the offset, although the scatter is not. The resulting CPSST algorithms for the dual window and split window combination of channels are as follows:

$$\left.\begin{aligned} \text{CPSST (3, 4)} &= \frac{0.117T_{11} - 31.64}{0.117T_{11} - 0.0559T_{3.7} - 15.92} \\ &\quad \times (T_{3.7} + 1 - T_{11}) + T_{11} \\ \text{CPSST (4, 5)} &= \frac{0.1761T_{12} - 47.56}{0.1761T_{12} - 0.117T_{11} - 15.72} \\ &\quad \times (T_{11} + 0.2 - T_{12}) + T_{12} \end{aligned}\right\}. \quad (8)$$

A CPSST triple-window solution of the form $T_{11} + \gamma_t[T_{3.7} - T_{12} + C]$ is obtained from a linear combination of the dual and split-window algorithms given above. The requirement that the coefficient of T_{11} be unity and that the coefficients of $T_{3.7}$ and T_{12} be equal in magnitude provides two linear equations in terms of the effective split-window and dual-window gamma coefficients, γ_s and γ_d given with (8). Solving this set of equations one obtains an effective triple window gamma parameter:

$$\gamma_t = \gamma_d(1 - \gamma_s)/(1 - \gamma_s - \gamma_d). \quad (9)$$

Again, the offset parameter C serves to minimize the scatter of the CPSST relative to the surface temperature. The final solution becomes

$$\text{CPSST (3, 4, 5)} = T_{11} + \gamma_t[T_{3.7} + 0.6 - T_{12}] + 0.4. \quad (10)$$

The constant term is included to remove the overall bias of the triple-window algorithm. It is interesting to note that (9) can be used to obtain the gamma parameter for the triple-window MCSST algorithm. The resulting value, 0.92, is very close to that obtained by linear regression, (7).

As an alternative to (10), any linear combination of (8) will provide a CPSST triple-window algorithm. A simple linear regression which minimizes the error of the CPSST solution relative to the surface air temperature measurements in the simulation dataset provides the following algorithm:

$$\text{CPSST (3, 4, 5)}^* = 0.34\ \text{CPSST (4, 5)} + 0.66\ \text{CPSST (3, 4)}. \quad (11)$$

A comparison of the accuracies achieved in simulation with this starred version and with the special form of triple window solution provided in (10) is given in Table 1, which is discussed in section 5. Because (10) generally provides the greater accuracy, it is the form of triple window solution that is applied in the remainder of this paper.

4. A variable gamma parameter

Equations (8) and (10) describe the CPSST solutions in terms of a gamma parameter that is a function of the two or three temperature measurements applied in the algorithms. It is instructive to evaluate these parameters as a function of a single temperature measurement (temperature dependence) and as a function of the two-channel temperature difference (water vapor dependence).

Figure 3 plots the gamma parameter for the split window, γ_s, the dual-window, γ_d, and the triple-window, γ_t algorithms as a function of the channel 4 (11 μm) brightness temperature measurements obtained

TABLE 1. Root mean square errors (°C)—simulation.

CPSST Algorithms	Noise free	Noise
Split	0.272	0.73
Dual	0.184	1.22
Triple	0.135	0.68
Triple*	0.137	0.84
MCSST Algorithms	**Noise free**	**Noise**
Split	0.326	0.82
Dual	0.206	1.98
Triple	0.081	1.16

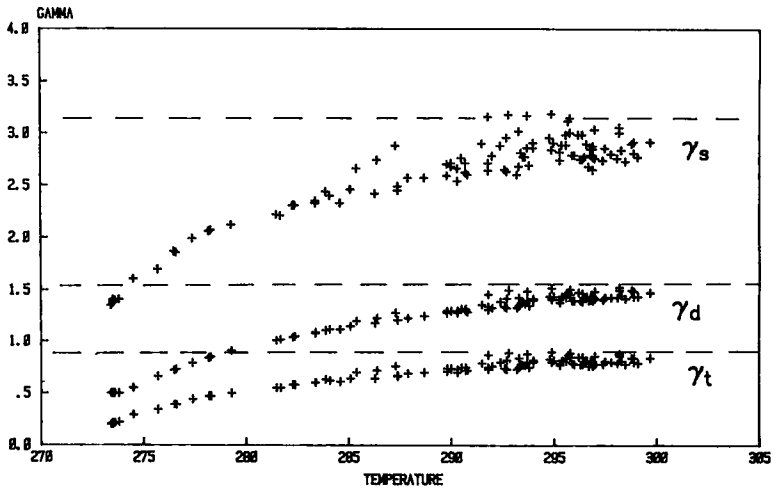

FIG. 3. The gamma parameters (γ_s, γ_d and γ_t) obtained, respectively, from the CPSST split-window, dual-window and triple-window algorithms as a function of the channel-4 brightness temperature. The brightness temperatures are obtained from simulation of the AVHRR Channels 3, 4, and 5. The dashed lines represent the corresponding MCSST gamma parameter values.

from the simulation dataset. The horizontal dashed lines represent the gamma parameters for the corresponding MCSST algorithms. Figure 4 plots the split-window gamma parameter as a function of the temperature difference (Channel 4 − Channel 5), which is a measure of the water vapor content of the atmosphere. Comparing these two figures, it is seen that below approximately 285 K, the CPSST parameters have primarily a temperature dependence and are considerably smaller than the corresponding MCSST gamma parameters, (7). At higher temperatures the parameters are sensitive to the water vapor content of the atmosphere and approach, as an upper limit, the corresponding MCSST values.

The water vapor or temperature difference dependence of the gamma parameters at high temperatures is critical for achieving the accuracies demonstrated in section 5 and is consistent with the results shown in Fig. 1 (see Introduction). The strong temperature dependence at low temperatures is not so easily explained in terms of a physical model of radiative transfer, but is a peculiarity of the CPSST solution that requires additional interpretation. As seen in Fig. 3, the gamma parameters of the dual-window and split-window algorithms drop rapidly with decreasing temperature, attaining a value of unity or less at sufficiently low temperatures. At this value, this solution, (6), becomes a single-channel measurement with an offset, T_i^*, or a

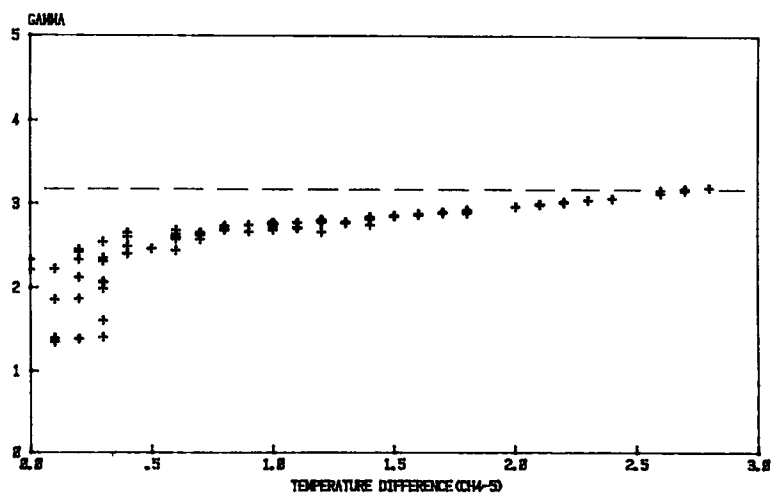

FIG. 4. As in Fig. 3 except for the gamma parameter obtained from the CPSST split-window algorithm as a function of the channel 4 minus channel 5 temperature difference.

simple average of two-channel measurements. In either case there is no correction for possible variations in water vapor absorption. Thus, at high temperatures the CPSST solutions correct for water vapor absorption with a two-channel temperature difference factor multiplied by a gamma parameter that is also a function of the temperature difference, whereas at low temperatures the water vapor is treated as a uniformly mixed gas, resulting in a single-channel algorithm. In a sense, the CPSST solutions account for the restrictive saturation upper limitation upon water vapor concentration at low temperatures. It is interesting that the dual-window algorithm transforms to a single-channel solution at a higher temperature than does the split-window algorithm, which relates to the fact that the 3.7 μm window channel is much less affected by water vapor absorption than are the 11 and 12 μm AVHRR channels. Further, the triple-window algorithm, (10), evolves to a single-channel solution only when its gamma parameter falls to zero. It is apparent from Fig. 3 that all of the gamma parameters would become negative at sufficiently low temperatures, which represents an undesirable extrapolation of the model. To avoid this problem, minimum thresholds for each of the gamma parameters should be established. If the gamma value falls below the threshold, it is reset to the threshold value. In the subsequent error analyses here, these thresholds are set at 1.0, 0.5 and 0.0, respectively, for the split-window, dual-window and triple-window CPSST algorithms.

The cause of the unrealistic values of the gamma parameter at sufficiently low temperatures is the linear form of the single channel algorithms, (4). Below a certain temperature, i.e., $T = 270$ K, this algorithm yields a surface temperature which is lower than the channel temperature measurement, which is unrealistic. It may be seen with (6) that the gamma parameter will become negative when the parameter $SST_j - T_j$ become negative. A nonlinear single channel algorithm could be defined to eliminate this problem.

5. Simulation error analysis

This section compares the errors within the dependent dataset in estimating sea surface temperature associated with the various algorithms derived previously. In this analysis the radiosonde-measured surface air temperature is the observed or "ground truth" temperature measurement. The root-mean-square error of the difference parameter (predicted minus observed temperature) for the various MCSST and CPSST algorithms is shown in Table 1. In general, it may be concluded that the MCSST and CPSST algorithms, although quite different in form, provide very similar accuracies and the standard deviations of the differences are quite small when the measurements are noise free.

Not included in the previous analysis is the effect of errors that are always present in satellite data. We distinguish here between channel correlative and non-channel correlative error sources. A familiar example of the former is cloud contamination while examples of the latter include instrumental noise, mis-registration between channels, and sunglint contamination. The effect of the latter types of error sources upon the SST algorithms is simulated by adding a value from the uniform random distribution into the radiance measurement of each channel. The magnitude of the random error is computer generated for each of the 110 AVHRR simulation brightness temperatures and added to the corresponding radiance value which is then converted back to temperature. The signal-to-maximum-error ratio (S/N) at 300 K in radiance units has been set at 20 and 200 for the 3.7, and 11 or 12 μm channels, respectively. This corresponds to a maximum error of approximately 1° and 0.3°C in these two window regions. These values do not represent an actual AVHRR instrument but are illustrative of the effects that can occur. The effect of the noise on the CPSST and MCSST triple-window algorithms is demonstrated with Figs. 5 and 6, in which are plotted the temperature errors under noise-free and noisy conditions, respectively. The temperature errors associated with the triple window MCSST algorithm under noisy conditions is much larger at low temperatures than at

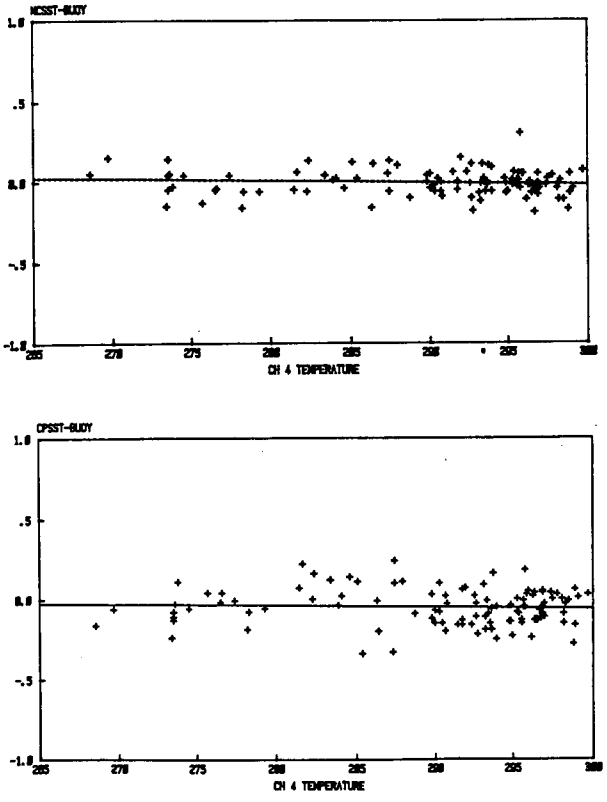

FIG. 5. The simulated temperature errors (algorithm minus the radiosonde surface temperature measurement) for both the MCSST and CPSST triple-window algorithms as a function of the channel 4 brightness temperature when no noise is included in the data.

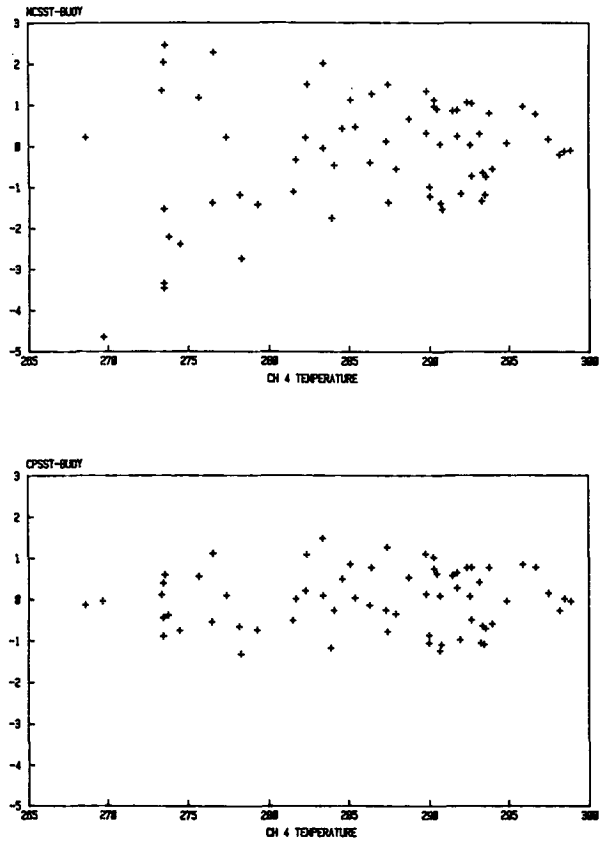

FIG. 6. As in Fig. 5 except for noise added to the channel 3 data. The signal-to-maximum noise ratio (S/N) of 20 applies at a temperature of 300 K.

high temperatures because the radiance-signal-to-noise ratio is a function of temperature. This is especially true for the 3.7 μm channel because the Planck function has a very strong temperature dependence at this wavelength ($B \propto T^{15}$) whereas the noise is independent of the scene temperature. Figure 6 shows that most of the error at low temperatures is removed with the CPSST algorithms. This rather dramatic improvement, which applies only with nonchannel correlative errors, occurs because the gamma parameter of the CPSST algorithms is much smaller in magnitude than that of the MCSST algorithms at low temperatures resulting in a lower sensitivity to noise. Similar results are obtained with the dual-window and split-window algorithms, and the error statistics associated with these algorithms when the measurements are noisy are also given in Table 1.

6. Analysis with real AVHRR data

The AVHRR instruments on the NOAA series satellites are designed to be exceptionally noise free, having noise equivalent temperature errors ($NE\Delta T$) of approximately 0.1°C at 300 K in the thermal infrared channels. Generally during the first few months of operation the instruments have exceeded this specification. Subsequently the 3.7 μm channel has become increasingly contaminated with a form of semicoherent electrical interference which eventually makes the 3.7 μm channel useless for quantitative sea surface temperature processing. As shown in Fig. 7, this process began in April 1982 with NOAA-7 and the interference

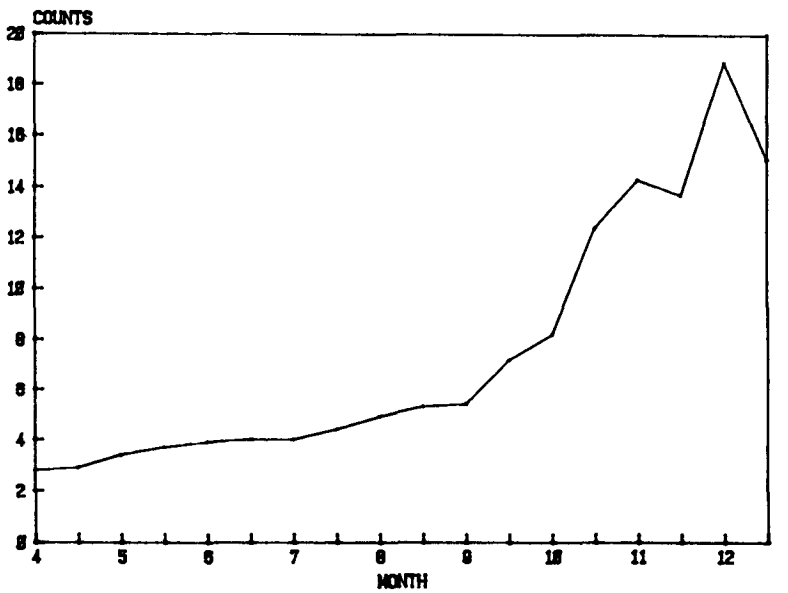

FIG. 7. The standard deviation of the channel 3 space-viewed scene in counts as a function of time. The biweekly values are obtained by averaging two or three daily mean values. One count ranges from approximately 0.15° to 0.05°C as the scene temperature increases from 0° to 30°C.

TABLE 2. Root mean square errors (°C)—AVHRR data.

CPSST Algorithms	Data 1982	Data 1983
Split	0.69	0.50
Dual	0.70	1.21
Triple	0.66	0.81
MCSST Algorithms	**Data 1982**	**Data 1983**
Split	0.71	0.62
Dual	0.69	1.89
Triple	0.63	1.30

increased throughout the year. The 1982 NOAA-7 data are, therefore, an excellent source for evaluating the ability of the CPSST algorithms to reduce the effects of instrumental noise relative to the MCSST algorithms.

A set of global area coverage (GAC) data having a nominal spatial resolution of 4 km and coincident temperature measurements from moored buoys were collected from January through March in 1982 and 1983. These buoys are concentrated along the east and west coasts of the United States, and only locations at latitudes north of 35 deg are included in the database in order to exclude any effects of the El Chichón Volcano eruption in April 1982 (Strong et al., 1982; Walton, 1985). Satellite data screening and preprocessing consisted of 1) the rejection of all daytime data to eliminate possible solar contamination in channel 3; 2) the rejection of all data with satellite zenith angles greater than 50 deg; 3) the rejection of satellite data that were cloud contaminated; 4) nine-sample channel averaging of the remaining data, which lowers the noise content of the 3.7 μm channel; and 5) data calibration to brightness temperatures in each of the three AVHRR channels.

Screening of nighttime cloud contamination in the AVHRR data consists primarily of a uniformity test. The original AVHRR data comprise 11 × 11 arrays of uncalibrated count values (4 km resolution) in each of the three window channels. The array is centered over the buoy and encompasses an area of approximately 50 × 50 km. The warmest channel 4 sample within each array is found. The uniformity test requires that the maximum channel 4 variation within the 3 × 3 subarray centered on this sample be no more than

TABLE 3. 1983 Buoy—AVHRR matchup data.

Buoy ID	Buoy Temp (k)	Buoy—Split MCSST	Buoy—Dual MCSST	Buoy—Split CPSST	Buoy—Dual CPSST
46024	288.8	0.8	0.8	0.1	0.4
46006	284.3	−0.5	3.1	−0.8	1.8
46010	283.4	0	1.6	−0.7	0.6
46006	284.6	−0.7	−1.4	−1	−1.4
46006	284.4	−0.9	−0.9	−1	−0.9
46004	279.6	−0.7	2.1	−0.7	1
44005	279.9	0.7	2.2	0.5	1.3
44005	279.9	0.8	2.5	0.7	1.5
46006	284.8	0	1.6	−0.2	1.1
46006	284.8	0.1	−0.4	−0.1	−0.3
46004	279.4	−0.1	0	−0.2	−0.1
C7L	282.3	1	1.7	0.6	1.2
C7L	282.3	0.8	1.1	0.5	0.8
46010	284.4	0.6	2.5	0.4	1.8
46004	279.4	0	1.3	−0.2	0.6
C7L	282.4	0.5	2.9	0.6	2.2
46006	284.3	0.7	−0.1	0.6	0.2
C7L	281.9	0.3	−2	0.2	−1.2
C7C	279.7	0.3	−0.5	−0.1	−0.4
C7C	279.7	0.7	−1	0.3	−0.4
46006	284.8	0	1.6	−0.2	1.1
46006	284.8	0.1	−0.4	−0.1	−0.3
44005	278.4	0.6	1	0.1	0.3
46010	284.8	1.1	0.5	0.9	0.7
46006	283.4	0.4	1.2	0.1	0.9
46006	283.7	1	1.2	0.3	0.7
C7C	278.5	0.8	0.6	0.3	0.2
46004	279.8	−0.1	−3.2	−0.4	−2.2
44005	278.8	0.8	−2.7	0.2	−1.7
C7R	285.2	0.5	−2.9	0.2	−2.3
C7C	278.6	0.5	3.9	0.1	1.6

two counts (approximately 0.2°C). If this requirement is satisfied, the nine-sample averages are computed for each channel and the data are converted to calibrated brightness temperatures. This uniformity test is very similar to that performed for global operational mapping of sea surface temperatures (McClain et al., 1985) and is very effective in detecting nonuniform or partly-cloudy conditions. Most uniform clouds are associated with unreasonably low temperature measurements, which are also rejected. Approximately nine-tenths of the original data are rejected with these various tests. It should be noted that the operational sea surface temperature product output which is archived globally could not be applied here. The NESDIS operational cloud tests assume noisy data are cloud contaminated and purges the data of interest in this study.

Remaining after all screening procedures is a 1983 dataset consisting of 31 matchups and a 1982 dataset comprising 42 matchups. The various MCSST and CPSST equations [i.e., (8), (9) and (10)] are computed for each of these datasets. With the real satellite data, however, we follow the operational procedure of performing a temperature-dependent bias correction to the algorithm values using an expression derived from an independent satellite/drifting buoy matchup dataset (Strong and McClain, 1984). Table 2 summarizes the error statistics for the 1982 and 1983 datasets. With the relatively noise-free 1982 data, both types of algorithms provide very similar accuracies. With the 1983 data the situation is quite different. The two split-window algorithms provide the highest accuracy since they do not use the noisy 3.7 μm data. Further, the CPSST dual-window and triple-window algorithms result in considerably less error than the corresponding MCSST algorithms. Table 3 contains the individual matchups in the 1983 dataset. Those cases in which the split-window algorithms provide accurate results while the dual-window algorithms are in error reflect the presence of noise in the 3.7 μm channel. In these cases the CPSST dual and triple-window algorithms provide approximately a 30–35% improvement over the corresponding MCSST algorithms. The dataset itself has a somewhat limited temperature range, between 5°–15°C. At higher temperatures the improvement provided by the CPSST algorithms would tend to be less, as would the magnitude of the MCSST errors since the signal-to-noise ratio would be greater. At temperatures below those present in this dataset, the tendency would be just the opposite.

In conclusion, a nonlinear, multiple-window algorithm for sea surface temperature has been developed graphically and justified physically in appendix A. The nonlinearity is described in terms of gamma parameter, γ, which varies with temperature and total atmospheric water vapor amount. This is in opposition to the usual linear algorithms, which are characterized by a constant gamma parameter. It is surprising that two such dissimilar algorithms provide nearly equal accuracies with both simulation data and real AVHRR data under noise-free conditions. When the satellite data contain a significant amount of noise, however, it has been demonstrated that the nonlinear CPSST algorithms greatly reduce its effect in all but very hot and humid atmospheres.

Acknowledgment. The author expresses appreciation to E. Paul McClain, Alan E. Strong and Dan Tarpley for reviewing this paper, and to Madelyn Bowman and Olivia Smith for preparing the final copy.

APPENDIX A

Physical Justification and Derivation of Nonlinear CPSST Algorithms

Following the formulation of Prabhakara et al., 1974, the radiative transfer equation can be written as

$$I(\nu) = B(\nu, T_s)\tau(\nu, P_s) + \bar{B}(\nu)[1 - \tau(\nu, P_s)], \quad \text{(A1)}$$

where $\bar{B}$ is a weighted mean Planck emission of the atmosphere, and T_s and P_s are the surface temperature and pressure and τ is the transmittance from the surface. The Planck function, B, can be expanded about T_s using a Taylor series to yield

$$T(\nu) = T_s + (\bar{T} - T_s)(1 - \tau), \quad \text{(A2)}$$

where $\bar{T}$ is a weighted mean atmospheric temperature. In the 11 to 12 μm region the primary atmospheric absorber is water vapor and (A2) may be expressed in terms of the water vapor absorption coefficient, $k(\nu)$,

$$T(\nu) = T_s - k(\nu)w[T_s - \bar{T}(\nu)], \quad \text{(A3)}$$

where w is path length of water vapor.

In terms of the wide band spectral split window channels of the AVHRR, i.e., channels i and j, (A3) becomes

$$\left.\begin{aligned} T_i &= T_s - k_i\beta_i \\ T_j &= T_s - k_j\beta_j \end{aligned}\right\}, \quad \text{(A4)}$$

where

$$\beta_i = w(T_s - \bar{T}_i).$$

The linear algorithm (1) is obtained from (A4) under the assumption that k_i and k_j are constant or at least have the same temperature dependence and that β_i equals β_j.

In general β_i and β_j vary with each atmosphere and cannot be obtained from the AVHRR data. We may, however, define an average $\bar{\beta}_i(T_i)$ which is independent of the atmosphere but is a function of the channel-i brightness temperature. A monochromatic value for this parameter could be derived by linear regression using a collection of atmospheric temperature and moisture radiosonde data in a transmittance model such as provided by Weinreb et al., 1980. However,

the proper procedure for estimating this parameter for wide band AVHRR channels is neither obvious nor necessary to the following development.

With (A4), this parameter defines a climatological surface temperature

$$\bar{T}_s = T_i + k_i\bar{\beta}_i(T_i) \tag{A5}$$

Since (4) and (A5) both define the climatological surface temperature in terms of a single-channel, brightness temperature, they may be equated to provide a temperature dependent absorption coefficient

$$k_i = (\mathrm{SST}_i - T_i)/\bar{\beta}_i(T_i). \tag{A6}$$

Although the magnitude and temperature dependence of k_i is not specified with (A6), since $\bar{\beta}_i$ is not given, the implication is that k_i and k_j do not have the same temperature dependence as is assumed in the linear model. Again, the actual temperature dependence of k_i does not affect the final result. A discussion of the temperature dependence of the water vapor absorption coefficients in the 11 to 12 μm spectral region is given in Prabhakara et al., 1974.

Substituting (A6) into (A4) yields

$$\left.\begin{aligned} T_i &= T_s - (\mathrm{SST}_i - T_i)\beta_i/\bar{\beta}_i(T_i)\\ T_j &= T_s - (\mathrm{SST}_j - T_j)\beta_j/\bar{\beta}_j(T_j)\end{aligned}\right\}. \tag{A7}$$

Making the assumption that $\beta_i/\bar{\beta}_i$ equals $\beta_j/\bar{\beta}_j$, and solving the set of linear equations (A7), one obtains (6) as a solution for T_s.

In summary, in contrast to the linear development, the nonlinear algorithm development does not require that the absorption coefficients k_i and k_j have identical temperature dependencies and it relaxes the requirement that β_i equals β_j to a requirement of proportionality.

APPENDIX B

A Regression Procedure for Deriving the Offset Temperature T_i^*

We seek to solve for the parameter c which minimizes the error associated with the dual and split window CPSST algorithms as defined with Eq. (6). The error is relative to ground truth measurements designated SST. For the nth comparison the following definitions apply:

$$\left.\begin{aligned} W_n &= \mathrm{SST} - T_j\\ X_n &= \mathrm{SST}_j - T_j\\ Y_n &= \mathrm{SST}_j - T_j + T_i - \mathrm{SST}_i\\ Z_n &= T_i - T_j,\end{aligned}\right\}, \tag{B1}$$

where i and j are the two AVHRR window channels. The method of least squares requires c to satisfy

$$\sum_n \left[W_n - \frac{X_n}{Y_n + c}(Z_n + c)\right]^2 = \text{minimum}. \tag{B2}$$

Performing the indicated algebra and then taking the derivative of the resulting expression with respect to the parameter c and equating to zero one obtains the following expression:

$$\sum_n (W_nX_nY_n - X_n^2Z_n)(Z_n - Y_n) = c\sum_n (W_nX_n - X_n^2)(Y_n - Z_n). \tag{B3}$$

In arriving at (B3), a factor $(Y_n + c)^3$ has been removed from the denominator of each term. Strictly this removal is only valid if Y_n is a constant. In fact, $y + c$ has a weak temperature dependence and is well behaved, i.e., does not pass through zero. Therefore the removal represents a reasonable approximation. When (B3) is applied to the set of 110 radiosonde profile data in order to compute c, one obtains values of 0.20 and 1.04 for the split and dual window algorithms, respectively, which are in excellent agreement with the values obtained by trial and error, and applied in (8).

REFERENCES

Dalu, G., C. Prabhakara and R. C. Lo, 1981: Improved accuracy of the remote sensing of sea surface temperature. *Oceanography from Space,* edited by J. F. R. Gower, 109–114.

McClain, E. P., 1981: Multiple atmospheric-window techniques for satellite-derived sea surface temperatures. *Oceanography from Space,* Plenum Press, 73–85.

——, W. G. Pichel and C. C. Walton, 1985: Comparative performance of AVHRR-based multichannel sea surface temperatures. *J. Geophy. Res.,* **90,** 11587–11601.

McMillin, L. M., and D. S. Crosby, 1984: Theory and validation of the multiple-window sea surface temperature technique, *J. Geophy. Res.,* **89,** 3655–3661.

Prabhakara, C., G. Dalu and V. G. Hunde, 1974: Estimation of sea surface temperature from remote sensing in the 11- to 13 μm window region. *J. Geophy. Res.,* **79,** No. 33, 5034–5044.

Schwalb, A., 1978: The TIROS N/NOAA A-G Satellite Series, *NOAA Tech. Memo. NESS 95,* U.S. Dept. of Comm., Washington, DC.

Strong, A. E., and E. P. McClain, 1984: Improved ocean surface temperatures from space—comparisons with drifting buoys. *Bull. of the Amer. Met. Soc.,* **65,** No. 2, 138–142.

——, A. Gruber and L. Stowe, 1982: radiative effects of the El Chichon volcanic eruption: preliminary results concerning remote sensing. *NASA Tech. Memo. TM-84959,* 4–1.

Walton, C. C., 1985: Satellite measurement of sea surface temperature in the presence of volcanic aerosols. *J. Climate Appl. Meteor.,* **24,** 501–507.

Weinreb, M. P., and M. L. Hill, 1980: Calculations of atmospheric radiances and brightness temperatures in infrared window channels of satellite radiometers. NOAA Tech. Report NESS 80, U.S. Dept. of Comm., Wash., DC.